International Journal of Thermophysics, Vol. 25, No. 4, July 2004 (© 2004)

Dual Critical Points and Related Phenomena in Simple Fluids from the Perspective of (Approximate) Renormalization Theory[1]

J. A. White[2,3] and K. P. Tewari[2]

It is known that some single component fluids can have coexisting low-density and high-density liquid phases with two, separate, gas–liquid and liquid–liquid, critical points. Such behavior is found both by experiments and in recent molecular-dynamics simulations performed for certain simple isotropic attractive pair potentials with softened repulsive cores. In the present investigation, a "global" renormalization group theory that was employed previously to make predictions for simple Lennard–Jones and square-well fluids over wide ranges of density and temperature, including the critical point, in reasonably good agreement with molecular dynamics and Monte Carlo simulations, is applied to simple shoulder potentials and to square-well potentials with softened repulsive cores. Results using this renormalization approach are compared with some previously reported results for a shoulder potential and expectations regarding dual critical points for water.

KEY WORDS: critical point; gas–liquid coexistence curve; global renormalization; liquid–liquid phase transition; square-well with repulsive shoulder.

1. INTRODUCTION

In a recent publication Ryzhov and Stishov [1] reported that a "liquid–liquid" phase transition appeared when they applied a second-order thermodynamic perturbation theory to a "collapsing hard sphere system," a system of hard spheres with purely repulsive and isotropic interactions.

[1]Paper presented at the Fifteenth Symposium on Thermophysical Properties, June 22–27, 2003, Boulder, Colorado, U.S.A.

[2]Department of Physics, American University, Washington, DC 20016-8058, U.S.A.
[3]To whom correspondence should be addressed. E-mail: jwhite@american.edu

0195-928X/04/0700-1005/0

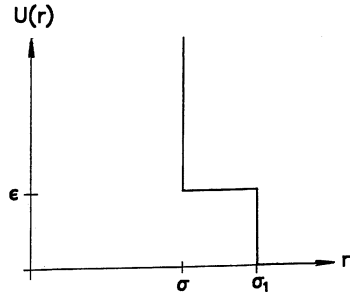

Fig. 1. Repulsive step pair potential, $U(r)$, Eq. (1), of Ryshov and Stishov [1]; σ is the hard-core diameter, σ_1 is the soft-core diameter, and ε is the height of the repulsive step.

The interaction potential they considered was that of a hard sphere, with a repulsive shoulder that extends out about 50% beyond the hard core (Fig. 1):

$$U(r) = \begin{cases} \infty, & r \leqslant \sigma, \\ \varepsilon, & \sigma < r \leqslant \sigma_1, \\ 0, & r > \sigma_1. \end{cases} \tag{1}$$

$$\sigma_1/\sigma \simeq 1.5,$$

where σ is the diameter of the hard sphere and r is the distance between the centers of two spheres. In particular, for number density $\rho = N/V$, temperature T, and pressure P expressed in units of $1/\sigma^3$, ε/k_B, and ε/σ^3, respectively, Ryzhov and Stishov found, for $\sigma_1/\sigma = 1.5$, a critical point at $\rho_c \simeq 0.985$, $T_c \simeq 0.21$, and (as can be inferred from their Fig. 2) $P_c \simeq 7.1$.

In another recent paper, Stanley and coworkers [2] discussed the possibility of a second critical point in water which may occur, according to simulations by Yamada et al. [3], at a temperature $T_{c2} \simeq T_{c1}/3$, pressure $P_{c2} \simeq 15P_{c1}$, and density $\rho_{c2} \simeq 3.5\rho_{c1}$. Here, and in the following, the subscript "c1" is used for the low-density critical point and "c2" for the high-density critical point. It had been shown in a somewhat earlier paper by Franzese et al. [4] that "liquid–liquid phase transition phenomena can arise solely from an isotropic pair interaction potential with two characteristic lengths." They considered in particular an isotropic pair potential which resembled the shoulder potential of Ryzhov and Stishov, but with an attractive square well extending for some distance beyond $r = \sigma_1$. In the notation of Franzese et al. [4] the potential (Fig. 2) had a hard-core

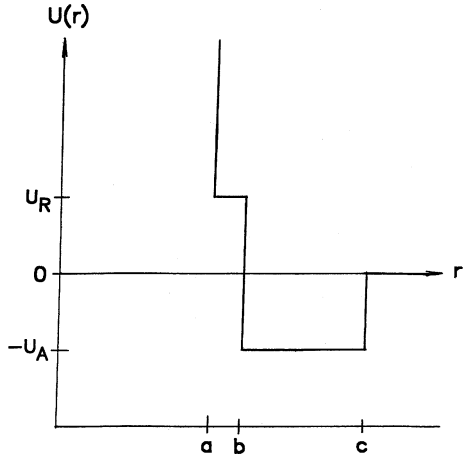

Fig. 2. Pair potential $U(r)$ in the presence of an attractive well, notation as in Ref. 4: distance a is the hard-core radius, b is the soft-core radius, and c is the cut-off radius. Energy U_A is the attractive energy, and U_R is the repulsive energy. (This figure is drawn to a different scale than in Fig. 1 of Ref. 4.)

radius a, a repulsive shoulder of radius $b > a$, and an attractive well from $r = b$ out to radius $r = c > b$. For $a < r < b$ the pair of particles repel each other with energy $U_R > 0$; for $b < r < c$ they attract each other with energy $-U_A < 0$. (Figure 2 is not drawn to the same scale as in Fig. 1 of Ref. 4.)

In Refs. 5–8 a "global" renormalization group theory was developed and applied to some simple isotropic Lennard–Jones and square-well pair potentials for which comparison could be made with results of molecular dynamics and Monte Carlo simulations. Agreement was found with simulations to accuracies of several percent. The question now arises: can the same renormalization methods be applied successfully to shoulder, and shoulder-next-to-well potentials? In particular, do the renormalization calculations give results in good or bad agreement with what has been reported by Ryzhov and Stishov for their repulsive shoulder potential [1] and suggested by Stanley and coworkers [2, 3] as a possibility for water?

The renormalization approach used here [5] and employed in Refs. 6–8, begins with a simple mean-field approximation, then includes corrections, not considered in the mean-field approximation, for fluctuations of density of increasingly long wavelengths, out to the longest wavelengths that make any appreciable contribution to the thermal properties of interest. The mean-field approximation begins with an expression for

the Helmholtz free energy per unit volume, $f_0(T, \rho)$, which yields the Carnahan–Starling [9] expression for the compression ratio, $Z = PV/RT$, for a gas of hard spheres. In a first, simplest approximation, the hard spheres are taken to have diameter $d = \sigma = a$. To the $f_0(T, \rho)$ is added the contribution of the repulsive (if any) and—when also a square well is present—attractive interactions, characterized by the shoulder height and width and well depth and width of the pair potential; in calculating this contribution the density distribution is assumed to be given by the pair correlation function $g_{\text{repulsive}}(T, \rho, r)$ for a gas of hard spheres in Percus–Yevick approximation [10] for spheres, in the first, simplest approximation, of diameter $d = \sigma = a$. The renormalization corrections then are made for local deviations (fluctuations) of density at all wavelengths, beginning with the shortest wavelengths that make appreciable contributions to thermal properties and continuing, doubling the fluctuation wavelength at each iteration of the renormalization procedure, until longer wavelengths make negligible contributions, even at the critical point.

The approximation that the spheres have diameter $d = \sigma = a$ was used successfully in Ref. 7, which treated simple square-well potentials. That approximation was not a good one for treating the Lennard–Jones potential, which has a sloping repulsive potential rather than one that rises abruptly to infinity at $r = \sigma$. For the Lennard–Jones potential, an "effective" hard-sphere diameter was used [6], employing an expression given by Barker and Henderson [11]. Here, in the spirit of that work, a second, less simple approximation also will be used, in which the diameter of the sphere for the pair correlation function and Carnahan–Starling approximation is given by

$$d(T) = \int_0^{\sigma_1 \text{ or } b} (1 - e^{-\beta U(r)}) dr, \tag{2}$$

where $\beta = 1/(k_B T)$. For work reported here, the $d(T)$ will also be used as the starting point for the calculation of contributions of the remaining portion of the repulsive shoulder and—if present—the square well, rather than using $d'(T) > d(T)$ for that starting point, as was done in Ref. 6. Results using $d'(T)$ intermediate between $d(T)$ and $\sigma = a$ can be expected to be somewhat, but not greatly, different near ρ_{c1}, T_{c1} from those presented here, but results near ρ_{c2}, T_{c2} may be more strongly affected.

The method of calculation used here is outlined in greater detail in Appendix A.

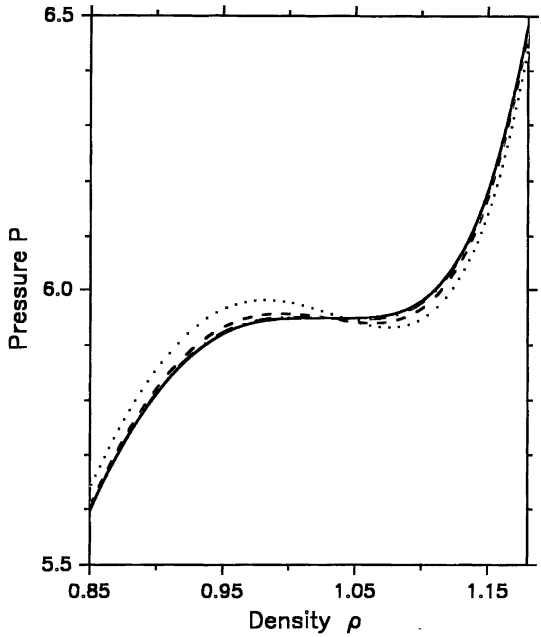

Fig. 3. Pressure isotherm for the repulsive step potential of Fig. 1 at critical-point temperature $T_c = 0.20$ in mean-field approximation, for $d = \sigma$, dotted line, and after $n =$ 1, 2, and 6 renormalizations [Appendix, Eq. (3)]: dashed, dash-dot (barely visible), and solid lines, respectively.

2. RESULTS

2.1. In the First, Simplest Approximation

For the shoulder potential, with $\sigma_1/\sigma = 1.5$, the mean-field approximation, for $d = \sigma$, gives a critical point at $\rho_c/T_c/P_c = 1.027/0.206/6.13$, compared with the values, mentioned earlier, $\rho_c/T_c/P_c \simeq 0.985/0.21/7.1$ reported by Ryzhov and Stishov [1]. Renormalization corrections at densities $\rho \sim 1$ are fairly small (Fig. 3). Including them, the critical point moves to $\rho_c/T_c/P_c \simeq 1.029/0.20/6.0$, exact values differing from these by as much as a couple percent depending on the precise choice made in the renormalization calculations for averaging volume and initial, shortest wavelength fluctuation (parameters $z \simeq 0.9$ and $\lambda_1 \simeq 6\sigma$ in Appendix A).

Results are quite sensitive to the diameter d assumed for the hard spheres in the calculation: if the d assumed in the pair correlation function, $g_{\text{repulsive}}(T, \rho, r)$, and Carnahan–Starling expression for hard spheres

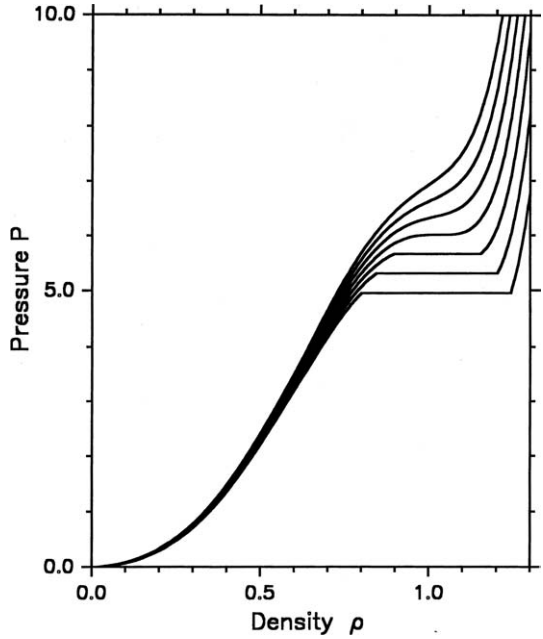

Fig. 4. Pressure isotherms, when $d=\sigma$, for the repulsive step potential of Fig. 1 at temperatures, from top to bottom, $T/T_c=1.3, 1.2, 1.1, 1.0, 0.9, 0.8, 0.7$.

is increased to 1% larger than the actual σ, i.e., $d=1.01\sigma$, then ρ_c, T_c, and P_c increase to approximately 1.05, 0.22, 6.6.

When, instead, the width of the shoulder is increased, so $\sigma_1/\sigma > 1.5$, then ρ_c, T_c, P_c all become smaller, with T_c decreasing to $T_c=0$ for $\sigma_1 \simeq 1.64$. Conversely, for a narrower shoulder, the ρ_c, T_c, P_c all increase, to $\rho_c/T_c/P_c \simeq 1.2/0.35/9.9$ when $\sigma_1/\sigma=1.40$.

Figures 4 and 5 include the critical isotherm (solid line in Fig. 3) and, in addition, several isotherms above and below T_c calculated for the same $\sigma_1/\sigma=1.5$. The horizontal lines for temperatures below T_c connect points on the coexistence curve with equal pressures and also equal chemical potentials, μ (where $\mu(T,\rho)=\partial f(T,\rho)/\partial\rho$). Unlike Fig. 2 in Ref. 1, Figs. 4 and 5 here do not show pressure isotherms at low temperatures crossing over higher temperature isotherms so as to lie above them at comparatively low densities.

When a square well is placed next to the shoulder, for example, in the notation of Ref. 4, for $b/a=1.5$ and $c/a=2.5$, then as U_A/U_R increases from zero (which gives results as quoted above for the shoulder potential),

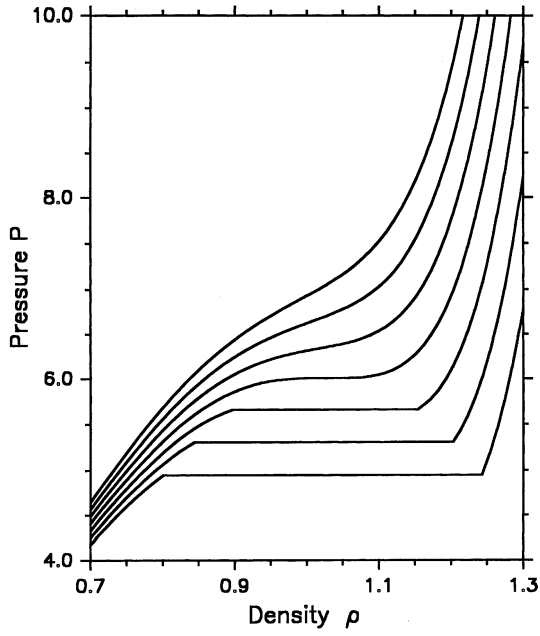

Fig. 5. Enlarged view of portion of Fig. 4 in the vicinity of the critical point.

the ρ_c and P_c decrease, while T_c increases, and, by the time U_A/U_R reaches 0.25, a *second* critical point has appeared, at very low density, temperature, and pressure: approximately, $\rho_c/T_c/P_c = 0.07/0.07/0.002$ for the new, low-density critical point, while the higher-density critical point has moved to $\rho_c/T_c/P_c \simeq 0.94/0.27/1.8$. Further deepening the well results in a rapid rise in the ρ_c, T_c, P_c of the new critical point, e.g., for $U_A/U_R = 0.4$ to approximately 0.16/0.53/0.022, while the high-density critical point moves to about 0.75/0.39/0.16, hence now has a lower critical point temperature than the "new", lower-density critical point. The pressure at the high-density critical point has dropped greatly; it becomes negative for $U_A/U_R > 0.45$.

In order to approximate expectations for water [2, 3], the ratio T_{c1}/T_{c2} should be about 3 and $P_{c2}/P_{c1} \simeq 15$, where the subscript "1" is for the low-density critical point and "2" for the high-density critical point. At $U_A/U_R = 0.4$, the P_{c2} increases rapidly as the outer extent of the attractive well is decreased: for $c/a = 2.3$ instead of 2.5, the low- and high-density critical points move to approximately 0.10/0.15/0.004 and 0.79/0.57/1.9, respectively. And then the ratio T_{c1}/T_{c2} increases if the shoulder width is

decreased: for example, for $b/a = 1.4$ when $c/a = 2.3$, the two critical points are at approximately 0.14/0.39/0.014 and 0.83/0.36/1.1. The above sets of numbers provide a feel for the sensitivity of the locations of the two critical points to the ratios c/a and b/a.

Continuing to deepen the well until $U_A/U_R = 1.0$, and simultaneously decreasing its width c/a (to keep $P_{c2} \gg P_{c1}$) and the shoulder's width b/a (to keep $T_{c1} > T_{c2}$), one arrives at $T_{c1}/T_{c2} \simeq 3$, $P_{c2}/P_{c1} \simeq 15$ for $c/a = 2.028$, $b/a = 1.2$ (as shown above in Fig. 2). Then the two critical points are located at close to $\rho_c/T_c/P_c = 0.19/1.63/0.070$ and 1.04/0.54/1.038. As indicated by the numbers mentioned in previous paragraphs, it is clear that the ratios T_{c1}/T_{c2} and P_{c2}/P_{c1} are quite sensitive to the precise choices of c/a and b/a. However, the ratio ρ_{c2}/ρ_{c1} is less so, and has ended up here substantially larger than the ratio $\rho_{c2}/\rho_{c1} \simeq 3.5$ mentioned in Ref. 3.

Figures 6–11 illustrate results, when $d = \sigma$, for the potential, as shown in Fig. 2, with $U_A/U_R = 1.0$, $c/a = 2.028$, $b/a = 1.2$. It will be noticed (Fig. 6) that renormalization corrections make a relatively large contribution for the low-density critical point, for which $P_{c1} \simeq 0.07$ is much smaller than the $P_c \simeq 7.1$ for the shoulder potential, and also (Fig. 7) that the vapor pressure, P_1, has dropped almost to zero already at $T_1 = 0.7T_{c1}$; it becomes negative for only slightly lower temperatures. The liquid side of the coexistence curve (which follows the "kinks" at high density in Fig. 7) looks like it may reach densities $\rho > 0.6$ at temperatures $< T_{c1}/3$. Figures 8 and 9 show that, somewhat like for the shoulder potential, the high-density critical point, with $P_{c2} \simeq 1.0$, has relatively little contribution from renormalization corrections, compared with what was seen for the low-density critical point, with $P_{c1} \simeq 0.07$, in Fig. 6. In Fig. 10 it is seen that the "vapor" pressure P_2, for the high-density, liquid–liquid coexistence curve, becomes negative below $T_2 \simeq 0.9T_{c2}$, and by temperature $T_2 = 0.8T_{c2}$ the low-density side of this coexistence curve extends already to somewhat below density $\rho = 0.7$. As this T_2 is equal to about $0.27T_{c1}$, that end of the coexistence curve for the liquid–liquid transition may extend to somewhat inside the lower-density, gas–liquid, coexistence curve, though not quite to the gas–liquid spinodal line [12]. It is also apparent from Fig. 10 that, especially at $T \leqslant 0.8T_{c2}$, the high-density end of the liquid–liquid coexistence curve extends to such high densities, i.e., to $\rho \geqslant 1.28$, that there may be serious doubts about assuming one then still has a liquid instead of a rather compact solid.

2.2. In a Less Simple Approximation

Results especially for temperatures around the second critical point change qualitatively when the simplest approximation, $d = \sigma = a$, for the

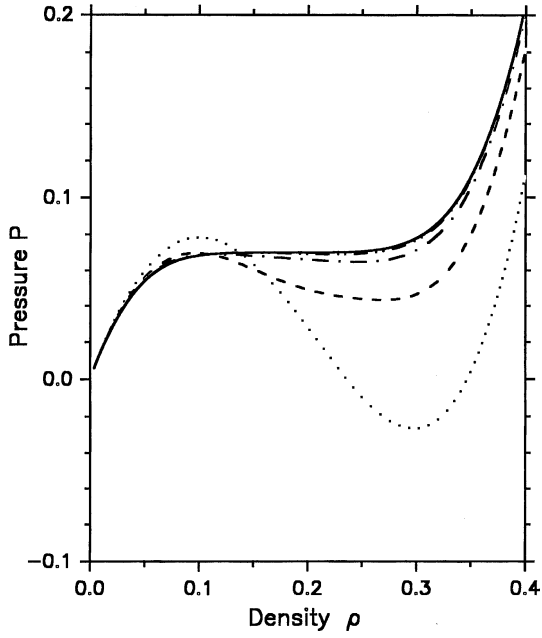

Fig. 6. Pressure isotherm, when $d = \sigma$, for the well-with-repulsive-shoulder potential of Fig. 2 at first critical-point temperature, $T_{c1} = 1.63$, in mean-field approximation, dotted line, and after $n = 1$, 2, 3, and 6 renormalization corrections [Appendix, Eq. (3)]: dashed, dash-dot, dash-dot-dot, and solid lines, respectively.

sphere diameter is replaced by $d = d(T)$ given by Eq. (2). Use of the $d(T)$ in Eq. (2) in place of $d = \sigma = a$ requires that the ratios b/a and c/a be increased and the shoulder height U_A/U_R decreased in order to have a second critical point at $T_{c1}/T_{c2} \simeq 3$, $P_{c2}/P_{c1} \simeq 15$, achieved, for example, by setting $U_A/U_R = 0.30$, $c/a = 2.214$, $b/a = 1.365$. This choice of parameters also makes $\rho_{c2}/\rho_{c1} = 4.08$, which is somewhat closer to the value 3.5 for this ratio estimated for water [3]. Calculated isotherms at the first, lower-density, higher-temperature gas–liquid critical point look qualitatively rather similar to those shown in Fig. 7, though with somewhat higher critical-point temperature; and they have renormalization corrections similar in size to those shown in Fig. 6. A comparison with experimental data for water [13] is shown in Fig. 11 for three calculated isotherms at and somewhat above and below the critical-point temperature. Agreement between theory and experiment at these temperatures is similar for the potential of Fig. 2 used in the $d = \sigma = a$ approximation in

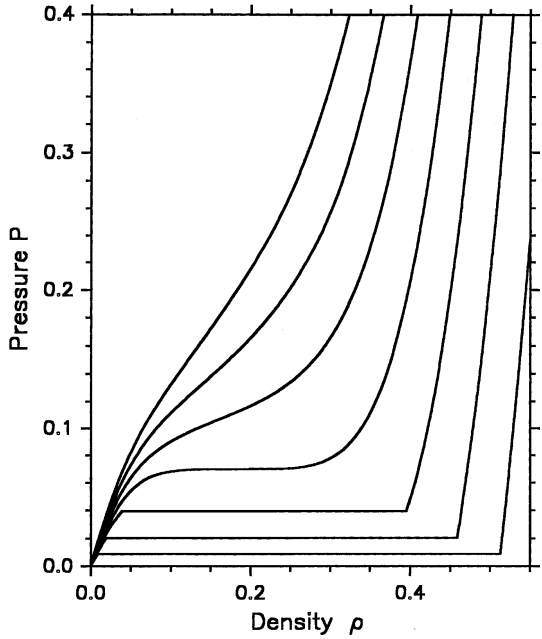

Fig. 7. Pressure isotherms, when $d=\sigma$, for the-well-with-repulsive-shoulder potential of Fig. 2 at temperatures around the first critical-point temperature; from top to bottom, $T/T_{c1}=1.3, 1.2, 1.1, 1.0, 0.9, 0.8, 0.7$.

Section 2.1. It may be of interest to note that at least as good agreement between theory and experiment at these temperatures is found for a simple square-well potential (square well without repulsive shoulder) of width $c/a=2.03$, though then there is no low-temperature, high-density, *second* critical point[14].

At the second critical point (higher density, lower temperature) using $d=d(T)$, the isotherms at temperatures below T_{c2} no longer, as in Section 2.1, lie neatly below one another as the temperature is decreased. Rather, for $U_A/U_R=0.30$, for temperatures below about $1.3T_{c2}$ the isotherms for decreasing temperature *increase* in pressure over a wide range of densities around ρ_{c2}, as shown in Fig. 12. Here, at constant pressure, the density decreases with decreasing temperature. (Possibly as pure coincidence, the temperature $1.3T_{c2}\simeq 0.429T_{c1}$, above which pressures, at, e.g., $\rho=0.75$, *increase* for increasing temperature, nearly coincides with 4 °C if, in practical units, $T_{c1}=647.1$ K, the gas–liquid critical point observed by experiment for water.) A coexistence curve, density versus temperature, below

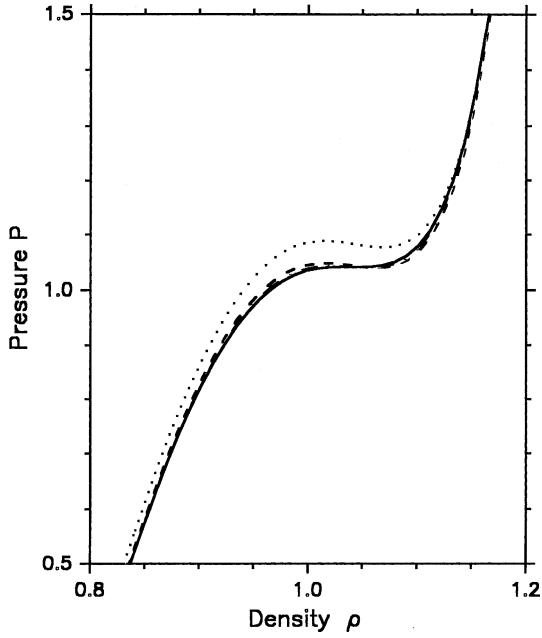

Fig. 8. Pressure isotherm, when $d=\sigma$, for the well-with-repulsive-shoulder potential of Fig. 2 at second critical-point temperature $T_{c2}=0.54$ in mean-field approximation, dotted line, and after $n=1$, 2, and 6 renormalization corrections [Appendix, Eq. (3)]: dashed, dash-dot (barely visible), and solid lines.

this liquid–liquid critical point is shown in Fig. 13, and the decrease in pressure as temperature rises for this coexistence curve (e.g., at $\rho \simeq 0.75$ in Fig. 12) is shown in Fig. 14. (The low-density, gas–liquid critical point, off scale in Fig. 14, is located at $T_{c1}=2.015$, $P_{c1}=0.087$.) The behavior in Fig. 14 seems to be qualitatively similar to that shown in Fig. 5 in Ref. 15.

It should be noted that the ρ, P, T behavior shown in Figs. 12–14 changes qualitatively if the shoulder height, $U_A/U_R=0.3$, is changed. In particular, for a height of $U_A/U_R<0.2$, and c/a and b/a adjusted to keep $T_{c1}/T_{c2} \simeq 3$, $P_{c2}/P_{c1} \simeq 15$, the pressures in Fig. 12 *decrease* with decreasing temperature, and the line in Fig. 14 tilts *upward* for increasing temperature. Also, results, qualitatively, are very sensitive to choices made for c/a and b/a which result in somewhat different values for T_{c1}/T_{c2} and P_{c2}/P_{c1} from those employed here. In particular, in some cases, e.g., for $U_A/U_R=0.30$, when $c/a=2.230$, $b/a=1.360$, the region of coexisting liquid–liquid phases closes up and disappears as the temperature drops sufficiently far below T_{c2},

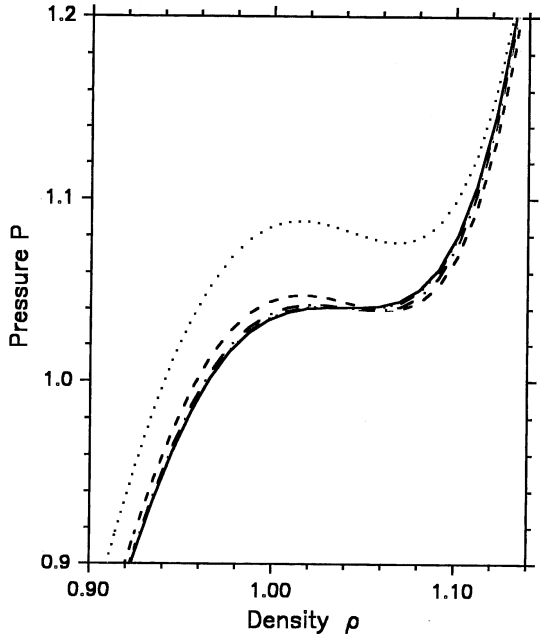

Fig. 9. Enlarged view of portion of Fig. 8 near the critical point, showing also the pressure isotherm after $n=3$ renormalization corrections (dash-dot-dot line, barely visible).

and then re-opens at a yet *lower* temperature, being an indication of a *third* critical point. In investigations completed to date, this seems not to be the case for choices of U_A/U_R, c/a, b/a that lead to the $P_{c2}/P_{c1} \simeq 15$, $T_{c1}/T_{c2} \simeq 3$ estimated for water [3].

Finally, use of Eq. (2) to determine the sphere diameter $d(T)$ for the shoulder potential *without* well (Fig. 1) makes a big difference for that potential. If the sphere diameter is gradually increased from σ toward $d(T)$, then the critical-point temperature drops rapidly relative to the critical-point pressure, and for the sphere diameter more than about 70% of the way from σ to $d(T)$ it seems not any more to be possible to find a critical point for the shoulder potential, even for a rather wide range of choices for its width, σ_1, and height ε. It is not known to the authors if this represents a failure of the method of calculation used here (for a rather wide shoulder, and no well). It would be of interest to have some molecular dynamics or Monte Carlo simulation results for this potential to compare with calculations being made here.

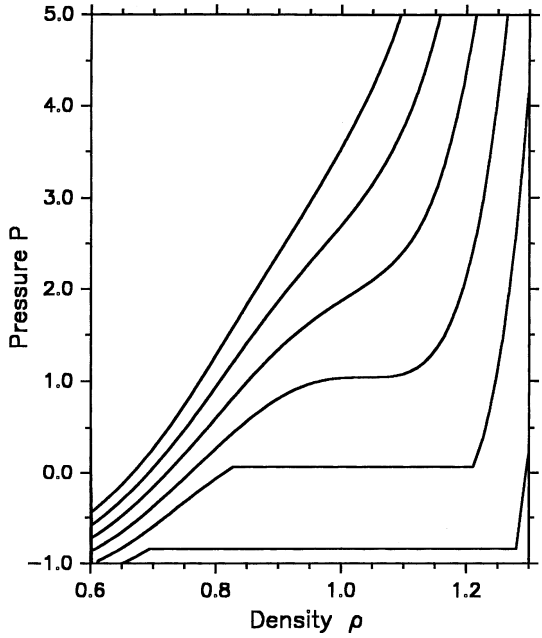

Fig. 10. Pressure isotherms, when $d = \sigma$, for the well-with-repulsive-shoulder potential of Fig. 2 at temperatures around the second critical-point temperature, where, from top to bottom, $T/T_{c2} = 1.3$, 1.2, 1.1, 1.0, 0.9, 0.8.

3. CONCLUSIONS

Proceeding from the simplest approximation (Section 2.1), in which a fluid of hard spheres with a repulsive shoulder potential is found to have a phase transition somewhat similar to that reported by Ryzhov and Stishov [1], the introduction of an attractive square-well potential beyond the repulsive shoulder results, as the well is deepened, in the appearance of a second, lower-density phase transition. Its critical point appears initially at a low critical-point temperature and pressure, then, as the well is deepened further, the critical-point temperature and pressure at low density rise, and the high-density critical-point pressure drops. A narrower well results in a higher critical-point pressure at high density; and a narrower repulsive shoulder causes the high-density critical-point temperature to drop, until, for at least one choice of shoulder width, well width, and ratio of well depth to shoulder height, the ratios of the low-density critical-point temperature and pressure to those at high density become

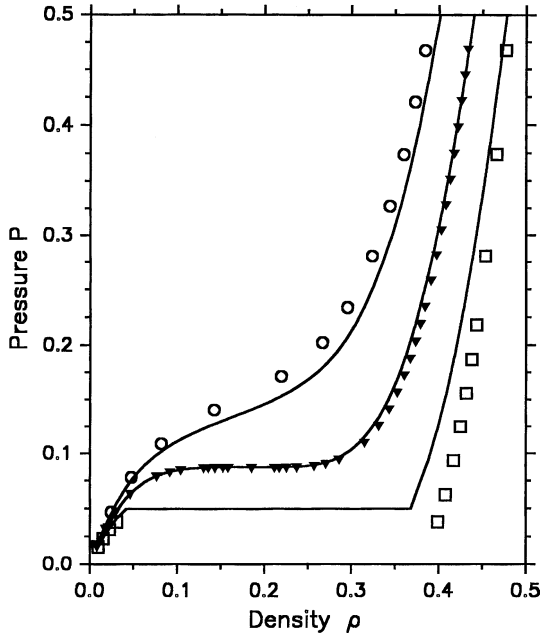

Fig. 11. Three isotherms near the gas–liquid critical-point temperature, T_{c1}, for water. Solid lines are calculated, for $d = d(T)$ given by Eq. (2), for $U_A/U_R = 0.30$, $c/a = 2.214$, $b/a = 1.365$ at temperatures $T/T_{c1} = 1.10$, 1.00, 0.90. Circles, triangles, and squares are for these same temperature ratios from experimental data for water [13], plotted for the choice of σ $(=a)$ and ε $(=U_A)$ that makes ρ_{c1} and T_{c1} given by theory and experiment agree at the gas–liquid critical point.

equal to ratios estimated for water in Refs. 2 and 3, assuming water indeed has dual critical points. The ratio of high-to-low critical-point densities obtained for this simple square-well potential with a repulsive shoulder is, however, substantially larger than was estimated [2, 3] for water.

Introducing a temperature-dependent sphere diameter [11] for use in the hard-sphere portions of the calculation (Section 2.2), much as was done successfully for a Lennard–Jones potential in Ref. 6, the low-to-high critical-point temperature and pressure ratios estimated for water [2, 3] were obtained for shoulders that are, in particular, 10–30% as high as the well is deep and somewhat wider than before. The ratio of high-to-low critical-point density, while still too large, is now closer to the value estimated for water [3]. Also, there may now appear, in the phase diagram,

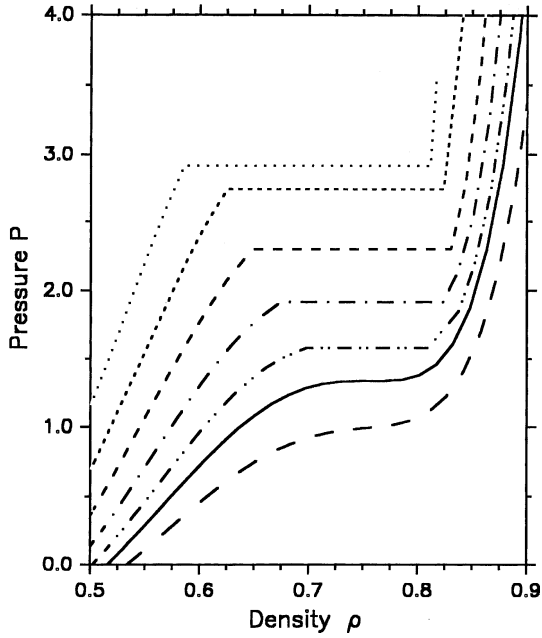

Fig. 12. Several calculated pressure isotherms at temperatures around the second (liquid–liquid) critical point, for the well-with-repulsive-shoulder potential used for Fig. 11. Temperatures, from bottom to top, $T/T_{c2} =$ 1.2, dashed line, 1.0, solid line, 0.9, 0.8, 0.7, 0.6, 0.5, dash-dot-dot to dotted line.

regions where density *increases* with increasing temperature at constant pressure. This is the case for shoulders more than about 20% as high as the well is deep. For some choices of shoulder height and width and well width, not too different from choices that give low-to-high critical-point temperature and pressure ratios similar to those estimated for water [3], the high-density phase behavior becomes even more complicated, with emergence of what appears to be a *third* critical point.

To the authors' knowledge, there are not as yet molecular dynamics or Monte Carlo simulations for either the simple repulsive shoulder or the attractive-well-with-repulsive-shoulder potentials considered here. Such simulations, if performed, could prove useful in testing the accuracy of the calculational methods employed here, as well as possibly help improve simple models for treating dual critical-point behavior, in water, in particular.

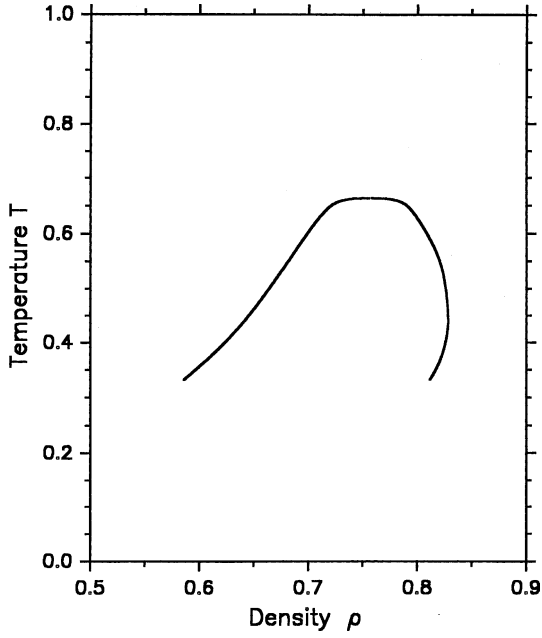

Fig. 13. Liquid–liquid coexistence curve for $T < T_{c2}$ isotherms, some of which are shown in Fig. 12.

APPENDIX: DETAILS OF THE CALCULATION

The renormalization method used was basically the same as that described in Ref. 5, and, in present notation, in Ref. 8, with the substitution in a few places of $d(T)$, Eq. (2), for σ. The following is a brief summary of the procedure. (In this appendix, unlike in the text and figures above, no assumption is made as to the units in which $\rho = N/V$, T, and P are expressed.)

The free-energy density, $f(T, \rho)$, of the fluid (Helmholtz free energy per unit volume) at temperature T and number density ρ is separated into hard core repulsive and repulsive shoulder plus any attractive parts. Beginning with $f_0(T, \rho) = f_{\text{repul}}(T, \rho)$, renormalization contributions are computed for increasingly long fluctuation wavelengths, beginning with wavelength λ_1. After n renormalizations ($n-1$ doublings of the initial fluctuation wavelength λ_1) the free energy density $f(T, \rho)$ is written as

$$f(T, \rho) \simeq f_n(T, \rho) - \rho^2 a(T, \rho), \tag{3}$$

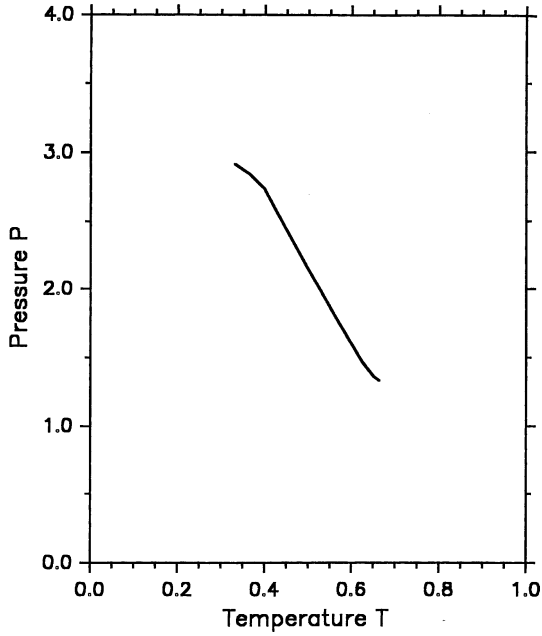

Fig. 14. Pressure versus temperature for the liquid–liquid coexistence curve in Fig. 13. The liquid–liquid critical point, Figs. 13 and 14, is located at $\rho_{c2}/T_{c2}/P_{c2} = 0.757/0.663/1.336$. The gas–liquid critical point, not shown in these figures, is at 0.185/2.015/0.087.

where, for each n (>0),

$$f_n(T, \rho) = f_{n-1}(T, \rho) + \delta f_n(T, \rho). \tag{4}$$

The $-\rho^2 a(T, \rho)$ is the contribution of the repulsive shoulder plus any attractive interactions to the free-energy density in the mean-field approximation (i.e., omitting any contributions resulting from fluctuations of density). The increment $\delta f_n(T, \rho)$ resulting from fluctuations of wavelength $\simeq \lambda_n$ is [16]

$$\delta f_n(T, \rho) = \frac{1}{\beta V_n} \ln \frac{I_{n,l}(T, \rho)}{I_{n,s}(T, \rho)}. \tag{5}$$

Here $\beta = 1/(k_B T)$, where k_B is Boltzmann's constant, V_n is the averaging volume, $V_n = (z\lambda_n/2)^3$, where $z \simeq 1$, and $I_{n,s}(T, \rho)$ and $I_{n,l}(T, \rho)$ are integrals over the amplitudes of the wave packets of density fluctuations of

wavelengths $\lambda \simeq \lambda_n = 2^{n-1}\lambda_1$:

$$I_{n,i}(T,\rho) = \int_0^{\rho'} dx\, e^{-\beta V_n D_{n,i}(T,\rho,x)}, \quad i = s, l. \tag{6}$$

In Eq. (6) the upper-density limit, ρ', is the smaller of ρ or $\rho_{\max} - \rho$, where $\rho_{\max}$ does not exceed the density of closest packing of the molecules. And each $D_{n,i}(T,\rho,x)$ is given by

$$2D_{n,i}(T,\rho,x) = \hat{f}_{n-1,i}(T,\rho+x) + \hat{f}_{n-1,i}(T,\rho-x) - 2\hat{f}_{n-1,i}(T,\rho), \tag{7}$$

where, for $i = l$,

$$\hat{f}_{n-1,l}(T,\rho) = f_{n-1}(T,\rho), \tag{8}$$

and for $i = s$,

$$\hat{f}_{n-1,s}(T,\rho) = f_{n-1}(T,\rho) - \rho^2 a_{\lambda_n}(T,\rho), \tag{9}$$

where

$$a_\lambda(T,\rho) = -\int_{r=d(T)}^{r=\infty} d\mathbf{r} \cos(\mathbf{k}\cdot\mathbf{r}) U_2(r) g_{\text{repul}}(T,\rho,r). \tag{10}$$

In Eq. (10) $g_{\text{repul}}(T,\rho,r)$ is the radial distribution function for the hard-core repulsive interactions, $U_2(r)$ is one half the remaining portion of the two-body potential (repulsive shoulder plus any attractive well), and $\mathbf{k}$ is the wave vector of the fluctuation of wavelength $\lambda = 2\pi/k$. In the limit $n \to \infty$, for which $\lambda_n \to \infty$, the $a_\lambda(T,\rho)$ becomes simply the $a(T,\rho)$ in Eq. (3).

The procedure summarized above is capable of determining, approximately, the free-energy density completely, by taking fully into account details of the intermolecular potential and contributions made by fluctuations at all wavelengths.

Specifically, the free-energy density $f_0(T,\rho) = f_{\text{repul}}(T,\rho)$ of a gas comprised of hard spheres of diameter d is, apart from a contribution to $f_{\text{repul}}(T,\rho)/\rho$ dependent on temperature but independent of density, approximately,

$$\frac{\beta f_{\text{repul}}}{\rho} = \frac{4y - 3y^2}{(1-y)^2} + \ln y, \tag{11}$$

where $y = (\pi\rho d^3)/6$. The pressure $P = \rho\partial f/\partial\rho - f$ calculated using $f = f_{\text{repul}}$ given by Eq. (11) yields, when multiplied by β/ρ, the Carnahan–Starling [9] expression for $Z = \beta P/\rho = PV/(RT)$ for hard spheres, namely,

$$Z_{\text{repul}} = \rho \frac{\partial}{\partial\rho}\left(\frac{\beta f_{\text{repul}}}{\rho}\right) = \frac{1 + y + y^2 - y^3}{(1-y)^3}. \tag{12}$$

In evaluating Eq. (10), the $g_{\text{repul}}(T, \rho, r)$ was approximated as that for a gas of hard spheres, of diameter d, in the Percus–Yevick approximation [10]. And the $U_2(r)$ was taken to be $U(r)/2$ of Eq. (1) and Fig. 1 for the repulsive shoulder potential, or including the well in Fig. 2, in case of the attractive well with repulsive shoulder. Once parameters σ, σ_1, and ε for the shoulder potential, or a, b, c, U_{R}, and U_{A} for the well with shoulder, and the parameters λ_1 and z internal to the RG theory, are specified, then the $f(T, \rho)$ given by Eq. (3) is completely determined—apart from a contribution (noted just before Eq. (11)) that depends only on temperature and does not contribute to the pressure—upon completion of n renormalizations. For the present calculations, the internal parameters λ_1 and z were assigned the values $\lambda_1 = 6\sigma$ and $z = 0.86$, respectively.

In the numerical calculations, the integrations were performed by the trapezoid rule, using equal size steps. Typically, 1000 steps were used for the calculation of each $a_\lambda(T, \rho)$, in Eq. (10). For the $g_{\text{repul}}(T, \rho, r)$ appearing in Eq. (10), the table in Ref. 10 was used, with interpolation when required. Equation (10) was evaluated for the 12 (dimensionless) densities $\rho\sigma^3 = 0.0, 0.1, 0.2, \ldots, 1.1$ for which tabulated values of g_{repul} were available [10], and a polynomial of fifth order in $\rho\sigma^3$ was fitted to each $a_\lambda(T, \rho)$ for use in Eq. (9), which needs to be evaluated at many intermediate densities in the range $0 < \rho\sigma^3 < 1.1$, and, for the shoulder potential and at low temperatures for the well with shoulder, to densities $\rho\sigma^3$ somewhat larger than 1.1.

For use in the present investigation, the free-energy density f was evaluated, at (dimensionless, $\rho\sigma^3$) density intervals of 0.0025, for $0 < \rho\sigma^3 \leqslant 1.35$; for the lower limit, a small value, $\rho\sigma^3 = 10^{-12}$, was used in place of $\rho\sigma^3 = 0$ to avoid the logarithmic singularity in Eq. (11). The integrand in Eq. (6) was evaluated, by the trapezoid rule, at the same dimensionless density intervals, 0.0025, using for the maximum integration limit $\rho'\sigma^3 = \rho_{\max}\sigma^3/2 = 1.35/2$. Larger choices for the upper limits of $\rho\sigma^3$ and $\rho'\sigma^3$ had almost no noticeable effect on the results obtained here. Four-point interpolation was used to estimate f when calculating thermal properties at densities intermediate between those at which f had been evaluated. Calculations of $f_n(T, \rho)$ were carried through to order $n = 6$. After the first few iterations of the recursion relations for increasing n, contributions δf_n decreased rapidly in size, with negligible contributions for present purposes except very close to the critical point for $n > 4$.

REFERENCES

1. V. N. Ryzhov and S. M. Stishov, *J. Exp. Theor. Phys.* **95:**710 (2002).

2. H. E. Stanley, M. C. Barbosa, S. Mossa, P. A. Netz, F. Sciortino, F. W. Starr, and M. Yamada, *Physica A* **315**:281 (2002).
3. M. Yamada, S. Mossa, H. E. Stanley, and F. Sciortino, *Phys. Rev. Lett.* **88**:195701 (2002). Other investigators, using different approaches, have arrived at appreciably different estimates for the temperature and pressure at the (conjectured) second critical point; see, for instance, S. B. Kiselev and J. F. Ely, *J. Chem. Phys.* **116**:5657 (2002) and results summarized there of some other alternative approaches.
4. G. Franzese, G. Malescio, A. Skibinsky, S. V. Buldyrev, and H. E. Stanley, *Nature* **409**:692 (2001). See also G. Malescio, G. Franzese, G. Pellicane, A. Skibinsky, S. V. Buldyrev, and H. E. Stanley, *J. Phys. Condens. Matter* **14**:2193 (2002).
5. J. A. White and S. Zhang, *Int. J. Thermophys* **19**:1019 (1998).
6. J. A. White, *J. Chem. Phys.* **112**:3236 (2000).
7. J. A. White, *J. Chem. Phys.* **113**:1580 (2000).
8. J. A. White, *Int. J. Thermophys* **22**:1147 (2001).
9. N. F. Carnahan and K. E. Starling, *J. Chem. Phys.* **51**:635 (1969).
10. G. J. Throop and R. J. Bearman, *J. Chem. Phys.***42**:2408 (1965).
11. J. A. Barker and D. Henderson, *J. Chem. Phys.* **47**:4714 (1967).
12. The spinodal line is where the slope of the chemical potential ($\mu = \partial f/\partial\rho$) vanishes, i.e., where $(\partial^2 f/\partial\rho^2)_T = 0$. A close look at the calculated results shows that at $T = 0.8T_{c2}$ the liquid–liquid coexistence curve does not extend quite as far as to the liquid side of the gas–liquid spinodal line.
13. E. W. Lemmon, M. O. McLinden, and D. G. Friend, in *Thermophysical Properties of Fluid Systems—NIST WebBook, NIST Standard Reference Database Number 69*, P. J. Linstrom and W. G. Mallard eds., National Institute of Standards and Technology, Gaithersburg, Maryland, http://webbook.nist.gov (March 2003).
14. K. P. Tewari, Ph.D. Dissertation, American University, Washington, D.C. (in preparation).
15. P. G. Debenedetti and H. E. Stanley, *Physics Today* **56**:40 (2003).
16. The subscripts l and s are (incorrectly) interchanged in Eq. (15) of Ref. 6 and Eq. (3) of Ref. 7, which otherwise are the same as Eq. (5) below, as well as in Eq. (10) in J. A. White, *J. Chem. Phys.* **111**:9352 (1999). This error was first noticed, and corrected, in proof, in Ref. 8. [The error originated when, in 1999, elegant notation introduced by L. Lue and J. M. Prausnitz in *J. Chem. Phys.* **108**:5529 (1998) was adopted without sufficient care, and, regrettably, also without acknowledging the source. I regret these mistakes and wish to apologize for them here.—J.W.]